Modeling Piezoelectric Actuators

Han J. M. T. A. Adriaens, Willem L. de Koning, and Reinder Banning

***Abstract*—The piezoelectric actuator (PEA) is a well-known device for managing extremely small displacements in the range from 10 pm (1 pm $= 10^{-12}$ m) to 100 μm. When developing a control system for a piezo-actuated positioning mechanism, the actuator dynamics have to be taken into account. An electromechanical piezo model, based on physical principles, is presented in this paper. In this model, a first-order differential equation is adopted to describe the hysteresis effect, and a partial differential equation is used to describe the mechanical behavior. Since, in practice, a PEA is most often used as an actuator for positioning mechanisms, we considered the influence of such a mechanism on the overall mechanical behavior of PEA and positioning mechanism together. For a well-designed mechanism, the overall mechanical behavior practically equals that of a single mass-spring-damper system, of which the undamped eigenfrequency and the relative damping can be designed favorably. With respect to traditional voltage steering, charge steering has the advantage that no hysteresis is encountered between electrical input and elongation. Electrical steering configurations for both cases of steering are presented. Finally, for the case of charge steering, we derived the total model of a piezo-actuated positioning mechanism. This model is dominated by the mechanical model, which could be designed favorably. Therefore, this model gives a broad range of possibilities for model-based controller design.**

***Index Terms*—Charge steering, distributed parameter system, hysteresis, piezo-actuated positioning, piezoelectric actuator.**

I. Introduction

THE piezoelectric actuator (PEA) is a well-known commercially available device for managing extremely small displacements in the range of 10 pm (1 pm $= 10^{-12}$ m) to 100 μm. The ratio of the input voltage and the output elongation is very favorable for this purpose. A disadvantage, however, is its highly nonlinear input/output behavior. More specifically, a PEA shows hysteresis behavior. In simple terms, this means that for a certain input, there is no unique output. Instead, the output depends on the input history. For high-accuracy positioning and tracking systems, the piezo-actuated positioning mechanism should be equipped with a controller. Modern controller design is based on a model of the system to be controlled. For piezo-actuated positioning mechanisms, the dynamical aspects of the PEA play a dominant role. In this paper, we focus on the modeling of the dynamics of a PEA as a standalone system and on the dynamics of a PEA and a positioning mechanism together.

A well-known description of PEAs was published in 1987 by a standards committee of the IEEE [20]. This description consists of two linear constitutive relations. Although this description is the most widely recognized one, we share the criticism in [11] that these relations fail to describe the hysteresis nonlinearity present in all PEAs and fail to describe the dynamical aspects of the actuator. Therefore, in this paper, this model is not considered anymore. In many other models, either only the linear dynamics or only the hysteresis nonlinearity is taken into account. Both types fail to describe one of the two important aspects. Therefore, although these models are sometimes used as a basis for control design, we consider them not accurate enough for our purposes. However, for the sake of completeness, we mention some references. Examples where only the linear dynamics has been modeled are, e.g., [6] and [18], and examples where only the hysteresis has been modeled are, e.g., [9], [10], [12], and [19]. In [23], the PEA has been modeled as a time-varying linear system where the time variance of the parameters is modeled by a neural network. A similar approach was mentioned in [13], where a self-tuning regulator is used to estimate the parameters of a linear model at every sampling instant. Recently, a model that consists of the series connection of a hysteresis operator and linear dynamics has been proposed in [5] and [8]. Although this model has no strong physical base, it seems an obvious choice for taking actuator nonlinearities into account. In both references, an approximate inverse hysteresis model has been used to cancel the hysteresis nonlinearity. In [15], the series connection of linear first-order dynamics and a hysteresis operator, i.e., the reversed order as above, has been used as a model for a so-called shape memory alloy actuator. In these actuators, hysteresis is encountered between temperature and elongation. In [2], a PEA model has been proposed, which differs only a little from the series connection of a hysteresis operator and linear second-order dynamics. In 1997, Goldfarb and Celanovic proposed a model for the PEA that is completely based on physical principles [11]. This model consists of both an electric and a mechanical domain, as well as the connection between the two domains. Furthermore, this model describes both the hysteresis nonlinearity and the linear dynamical aspects. In this section, we introduce more accurate and better applicable hysteresis and dynamical models than those proposed by Goldfarb and Celanovic [11] for use in their overall electromechanical model. From the very beginning of applying piezoelectric materials as actuators, they are voltage steered, and this is still the standard way of electrical steering. However, in the early 1980's, it has been independently reported in [4] and [17] that, in case of charge steering of PEAs, no hysteresis behavior is encountered. Based on the early and more

Manuscript received September 9, 1998; revised August 19, 1999. Recommended by Technical Editor K.-M. Lee. This work was supported by the Dutch Technology Foundation.

H. J. M. T. A. Adriaens was with the Faculty of Information Technology and Systems, Delft University of Technology, 2628 CD Delft, The Netherlands. He is now with ASM Lithography, 5500 AH Veldhoven, The Netherlands.

W. L. de Koning is with the Faculty of Information Technology and Systems, Delft University of Technology, 2628 CD Delft, The Netherlands (e-mail: w.l.dekoning@twi.tudelft.nl).

R. Banning is with the Faculty of Applied Sciences, Delft University of Technology, 2628 CD Delft, The Netherlands.

Publisher Item Identifier S 1083-4435(00)11061-0.

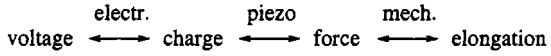

Fig. 1. Schematic representation of the different relations in a PEA.

recent literature on charge steering of PEAs, we present the basic principle of a charge-steering configuration. Furthermore, we consider the influence of a positioning mechanism on the overall dynamical behavior of a PEA and a positioning mechanism together. For a positioning mechanism that may be modeled with a mass-spring-damper system, we consider this influence in detail.

In Section II, some physical properties are discussed and an electromechanical model is presented. For the larger part, this model is due to [11]. In Section III, the differential equation describing the hysteresis phenomenon is introduced. A partial differential equation (PDE) as a mechanical model is derived and analyzed in Section IV. In Section V, the PEA is applied to a positioning mechanism and the influence of this mechanism on the mechanical model is analyzed. Basic configurations for both voltage and charge steering are introduced in Section VI. In Section VII, we consider the total model of a piezo-actuated positioning mechanism for the case of charge steering. Finally, in Section VIII, some conclusions are drawn.

II. Physical Background and an Electromechanical Model

Dielectric materials are insulators, thus, there is an electrical relation between electrical voltage and electrical charge. Piezoelectrics are a special type of dielectric in the sense that, in piezoelectric materials, an externally applied force induces an electrical charge. Conversely, an applied electrical charge induces a force. The former effect is known as the piezoelectric effect and was discovered in 1880 by the Curie brothers. The latter effect is the inverse piezoelectric effect. The word "piezo" derives from the Greek word "piezen," which means "to push." The effect was discovered when a pushing force or, in other words pressure, was applied to the material. In the beginning, both pressure electricity and piezoelectricity were used to describe the same phenomenon. Besides the piezoelectric and inverse piezoelectric effect, we have the already mentioned electrical relation between voltage and charge, and a mechanical relation between force and elongation. In Fig. 1, a schematic representation of the different relations is given. The piezo effect is the connection between the electrical and mechanical domains. Due to this effect, piezoelectrics are potentially useful as electromechanical actuators.

In naturally occurring piezoelectric materials, such as quartz, the (inverse) piezoelectric effect is too small to be of practical use. Man-made piezoelectric polycrystalline ceramics are much more suitable for actuator purposes because the useful properties, such as maximum elongation, can be influenced by the proper mixture of ingredients. A disadvantage of man-made piezoelectric ceramics is that a hysteresis effect is encountered between electrical voltage and electrical charge. Since only man-made ceramics are useful for actuator purposes, they are meant when we talk about PEAs. The piezoelectric effect (or the piezo effect for short) and the hysteresis effect play an important role in the dynamical behavior of these actuators.

TABLE I
Differences Between Voltage and Charge Steering

	Closed	Open
Steering source	voltage	charge
Resistance of source	0	∞
Hysteresis effect	yes	no
Piezo effect	yes	yes

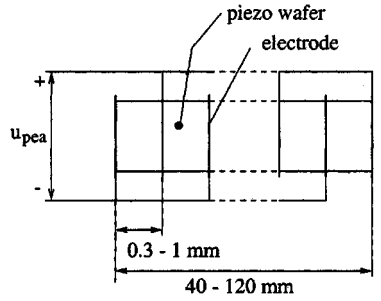

Fig. 2. Schematic representation of the stacked configuration of a PEA.

It is apparent from the scheme in Fig. 1 that, between charge and elongation, no hysteresis effect is encountered because, as mentioned, this effect is encountered between voltage and charge. Equally obvious, the hysteresis effect is encountered between voltage and elongation. The former situation can be realized by charge steering, while the latter situation occurs for voltage steering. Voltage and charge steering may be realized by a voltage and charge source, respectively, which have an internal resistance zero and infinite, respectively, and which may be called the (galvanically) closed and (galvanically) open situation. In both cases of steering, a charge is induced on the electrodes of the PEA. In the case of voltage steering, the hysteresis effect is present between voltage and charge. The electrical charge induces a force and, as a result, an elongation of the ceramic. This means that the piezo effect is present for both cases of electrical steering. All of this is summarized in Table I.

The most widely spread PEA configuration is the stacked one, of which a schematic representation is given in Fig. 2. Such a PEA stack consists of the series connection of a number of piezo wafers with an electrode between every two wafers. Clearly the wafers are in series mechanically and in parallel electrically. The latter is done in order to strengthen the effect of the individual wafers. The piezo wafers have a thickness of 0.3–1 mm. For maximum elongation ranging from 10 to 100 μm, the length of a PEA ranges from approximately 40 to 120 mm, respectively. $u_{\rm pea}$ is the voltage over every piezo wafer and over the total PEA.

As mentioned in Section I, a fairly accurate overall electromechanical model of a PEA is given in [11]. It is reproduced in Fig. 3. Here, the hysteresis and piezo effect are separated. H represents the hysteresis effect and u_h is the voltage due to this effect. The piezo effect is represented by $T_{\rm em}$, which is an electromechanical transducer with transformer ratio $T_{\rm em}$. The capacitance C represents the sum of the capacitances of the individual piezo wafers, which are electrically in parallel. The total current flowing through the circuit is $\dot{q}$. Furthermore, q may be seen as the total charge in the PEA. The charge q_p is the transduced charge from the mechanical side. The voltage u_p is due

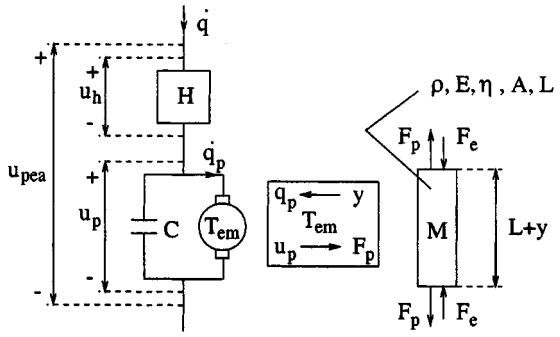

Fig. 3. Electromechanical model.

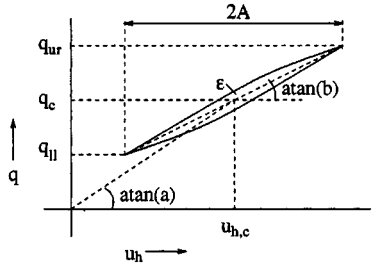

Fig. 4. Realistic hysteresis loop.

to the piezo effect. The total voltage over the PEA is $u_{\rm pea}$. The force F_p is the transduced force from the electrical side. The force F_e is externally applied. In practice, this is most often a pushing force. The resultant force $F_p - F_e$ mechanically drives the piezo material. The resulting elongation of the PEA is denoted by y. The mechanical relation between F_p and y is denoted by M. Note that we have equal electrical and mechanical energy at the ports of interaction, i.e., $u_p q_p = F_p y$. The piezo material has elasticity modulus E, viscosity η, and mass density ρ. Furthermore, the geometrical properties of the PEA are length L and cross-sectional area A. Mass m_p, stiffness k_p, and damping coefficient c_p can be calculated from the material and geometrical properties as follows:

$$m_p = \rho A L \tag{1}$$

$$k_p = \frac{EA}{L} \tag{2}$$

$$c_p = \frac{\eta A}{L}. \tag{3}$$

The complete set of electromechanical equations is as follows:

$$u_{\rm pea} = u_h + u_p \tag{4}$$

$$q = H(u_h) \tag{5}$$

$$q = C u_p + q_p \tag{6}$$

$$q_p = T_{\rm em} y \tag{7}$$

$$F_p = T_{\rm em} u_p \tag{8}$$

$$y = M(F_p - F_e) \tag{9}$$

where H and M represent the hysteresis and mechanical operators, which are discussed in Sections III and IV, respectively. Since in a PEA the individual piezo wafers are mechanically in series, it is to be expected that the longitudinal dynamics play an important role in the mechanical operator. It is well known that this often leads to a PDE model. Furthermore, because the individual piezo wafers are electrically in parallel, it is very accurate to take the sum of the capacitances of the individual wafers as electrical model, resulting in the capacitance C in (6).

The transduced force F_p is, in fact, present in every piezo wafer. However, because every wafer tends to elongate, the forces at the connection of two wafers cancel out. Therefore, macroscopically there are only forces at the first and last electrodes, as in Fig. 3.

III. Hysterics Model

In this section, we consider the hysteresis operator of (5), which is part of the total electromechanical model of (4)–(9)

By definition, a hysteresis effect is dynamic, rate-independent, and nonlinear. By rate-independent, we mean independent of the time scale. In [11], this effect is modeled by a combination of elementary elements. Therefore, the number of parameters in this model is relatively large. Furthermore, such a model is not very suitable for controller design purposes. Therefore, in [1], a differential equation, with only three parameters, is used as a hysteresis model. A differential equation is also more attractive when we want to use the model as a basis for controller design. In this section, we consider this equation in more detail. However, in [1], a much more extensive discussion may be found.

A hysteresis loop is defined as the stationary loop in the input/output plane for a quasi-static monotone oscillating input, e.g., a low-frequency sinusoid.

The equation under consideration is a first-order differential equation, which is proposed in [3]. It has been developed to describe magnetic hysteresis, but in [1], it has experimentally been verified that this differential equation is also suitable for describing electric hysteresis such as in a PEA. The model for the hysteresis effect between u_h and q is given by

$$\dot{q} = \alpha |\dot{u}_h| \left(f(u_h) - q \right) + \dot{u}_h g(u_h) \tag{10}$$

where $f(u_h)$ and $g(u_h)$ are functions with which you can "shape" the hysteresis loop. In [1], it has been proven that, for a sinusoid with offset $u_{h,c}$, the center point of a hysteresis loop is given by $q_c = f(u_{h,c})$. Furthermore, it has been proven that the average slope of a hysteresis loop is equal to $g(u_{h,c})$.

In theory, PEAs show lengthening saturation. In practice, however, we stay far away from saturation, i.e., we deal with hysteresis loops that are similar in shape to the one in Fig. 4. Therefore, the functions $f(u_h)$ and $g(u_h)$ may be chosen as

$$\begin{aligned} f(u_h) &= a u_h \\ g(u_h) &= b \end{aligned} \tag{11}$$

where a and b are constants.

Using the previously mentioned results, the equations for the center point and the average slope of a hysteresis loop are given by

$$q_c = a u_{h,c} \tag{12}$$

$$q_{ur} - q_{ll} = b 2A \tag{13}$$

where q_{ur} and q_{ll} are the upper right- and lower left-hand-side points of a hysteresis loop, respectively, and A is the input amplitude.

In (10) and (11), there are three independent parameters, namely, α, a, and b. This means that there should be three independent characteristic quantities in a hysteresis loop. Besides the center point and the average slope in [1], a relation has been derived for the hysteresis area ε for relatively small amplitudes of the sinusoidal input (Fig. 4)

$$\varepsilon = \frac{4}{3}(a-b)\alpha A^3. \tag{14}$$

Having experimentally determined a and b from center points and average slopes, the parameter α can then be experimentally determined from hysteresis areas.

For decreasing input amplitudes, it follows from the previous expression that, because of the power three, the hysteresis area decreases faster. This has first been noted in [7]. As a result, for small deviations from a center point, the hysteresis nonlinearity is well approximated by its average slope

$$\Delta q = b\Delta u_h \tag{15}$$

where Δ is used to indicate that we deal with deviation variables. This approximation allows for linear analysis of the total model.

In [1], it has been proven that for physically correct hysteresis, i.e., convergence to hysteresis loops and counterclockwise orientation and monotony of hysteresis loops, it is required that $\alpha > 0$ and that $0 < (1/2)a \leq b \leq a$.

IV. Mechanical Model

In this section, we consider the mechanical operator of (9), which is part of the total electromechanical model of (4)–(9).

In [11], the mechanical behavior is modeled by a single mass-spring-damper system. In a Bode plot, such a system only shows one peak, while experimental results in [6] indicate that there are many more peaks and valleys in between every two peaks. However, in the model in [6], only two peaks and one valley are taken into account. In fact, there are infinitely many peaks and valleys because the PEA is, in fact, a distributed parameter system, i.e., the mass of the PEA is not concentrated in some points, as in linear mass-spring-damper systems of arbitrary order, but the mass is distributed over the element. Such a distributed parameter system may be modeled by a PDE. The PDE for the case that damping is not taken into account is well known and can be found in every standard textbook on PDEs. This is not the case when damping is taken into account. In [14] and [22], PDEs were used to describe the mechanical behavior of the PEA where damping is accounted for. However, in both of these references, the damping has not correctly been modeled. Therefore, we derive a PDE ourselves. Since the individual piezo wafers are mechanically in series, it was, as mentioned in Section II, to be expected that the longitudinal dynamics would play an important role, which leads to a PDE model for the mechanical behavior.

As a first step in the derivation of the PDE, we derive the equation of motion. To this purpose, we consider Fig. 5, where

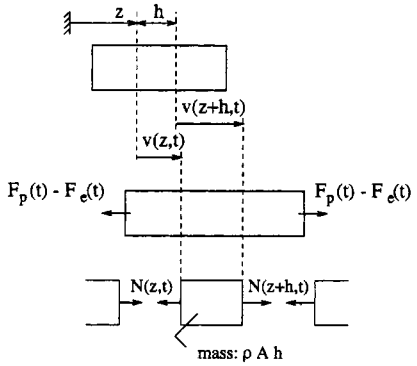

Fig. 5. PEA in undeformed and deformed state.

the PEA is shown in the undeformed and deformed states. The position variable of a piezo slice is z, while h is the thickness of a slice. At position z, we have that $v(z, t)$ and $N(z, t)$ are the displacement and the so-called normal force, respectively.

The impulse balance for a piezo slice can easily be obtained from Fig. 5

$$N(z+h, t) - N(z, t) = \rho A h \frac{\partial^2 v(z, t)}{\partial t^2}. \tag{16}$$

Dividing by h and taking the limit for h to zero gives the equation of motion

$$\frac{\partial N(z, t)}{\partial z} = \rho A \frac{\partial^2 v(z, t)}{\partial t^2}. \tag{17}$$

Secondly, we have to specify the material behavior. The relation by which this is specified is the constitutive relation, which solely depends on material quantities like E and η. Therefore, the constitutive relation is formulated in terms of stress σ and strain ε, of which the definitions are

$$\sigma(z, t) = \frac{N(z,t)}{A} \quad \varepsilon(z, t) = \frac{\partial v(z, t)}{\partial z}. \tag{18}$$

As a fairly accurate constitutive relation for many solids, among which the piezo ceramics, we take the Kelvin–Voigt model. It consists of the parallel connection of a spring element obeying Hooke's law and a viscous element behaving like a Newtonian flow. Mathematically, the model is given by

$$\sigma(z, t) = E\varepsilon(z, t) + \eta \frac{\partial \varepsilon(z, t)}{\partial t}. \tag{19}$$

Based on (18) and (19), the following relation for the normal force N can be derived:

$$N = EA\frac{\partial v}{\partial z} + \eta A \frac{\partial^2 v}{\partial z \partial t} \tag{20}$$

where the arguments z and t are omitted for notational convenience. Using the equation of motion and the equation for the normal force, i.e., (17) and (20), the PDE describing the mechanical PEA behavior can be derived to be

$$E\frac{\partial^2 v}{\partial z^2} + \eta \frac{\partial^3 v}{\partial z^2 \partial t} = \rho \frac{\partial^2 v}{\partial t^2}. \tag{21}$$

An alternative formulation can be found by using the definitions of mass, stiffness, and damping coefficient, i.e., (1)–(3)

$$k_p L\frac{\partial^2 v}{\partial z^2} + c_p L\frac{\partial^3 v}{\partial z^2 \partial t} = \frac{m_p}{L}\frac{\partial^2 v}{\partial t^2}. \tag{22}$$

Here, we are not interested in the analytic solution of the PDE for a specific input. Instead, our main interest is in the eigenmodes and corresponding eigenfrequencies and relative dampings. In order to determine these, it suffices to consider the free response ($F_p - F_e = 0$).

Systems described by a PDE are said to be infinite dimensional because infinitely many eigenmodes can be distinguished. The free response can be written as the infinite sum of the eigenmodes

$$v(z, t) = \sum_{i=1}^{\infty} v_i(z, t). \tag{23}$$

Each eigenmode is determined using the principle of separation of variables, i.e., its expression is taken to be of the following form:

$$v_i(z, t) = Z_i(z)T_i(t). \tag{24}$$

Substitution of this form in the PDE of (22), after some manipulations, gives

$$\frac{Z_i''}{Z_i} = \frac{\ddot{T}_i}{L^2\frac{c_p}{m_p}\dot{T}_i + L^2\frac{k_p}{m_p}T_i} \tag{25}$$

where "accent" and "dot" refer to derivatives with respect to z and t, respectively. The left- and right-hand side only depend on z and t, respectively, and, thus, the above equality is a constant, which is denoted by $-\mu_i^2$. The following two ordinary differential equations can now be derived:

$$Z_i'' + \mu_i^2 Z_i = 0 \tag{26}$$

$$\ddot{T}_i + \mu_i^2 L^2\frac{c_p}{m_p}\dot{T}_i + \mu_i^2 L^2\frac{k_p}{m_p}T_i = 0. \tag{27}$$

We start determining the amplitude of the eigenmodes, i.e., we consider (26), of which the general solution is given by

$$Z_i(z) = A_i\cos(\mu_i z) + B_i\sin(\mu_i z). \tag{28}$$

By specifying the boundary conditions, the constants can be determined. For instance, consider the practical situation where at $z = 0$ and $z = L$ the PEA is fixed and free, respectively. The displacement at $z = 0$ is given by $v_i(0, t) = Z_i(0)T_i(t)$. At a fixed end, the displacement equals zero for all t and, therefore, $Z_i(0) = 0$. Using this, the constant A_i can be determined as follows:

$$v_i(0, t) = 0 \;\rightarrow\; A_i = 0. \tag{29}$$

From (1)–(3), (20), and (24) the normal force at $z = L$ can be derived to be given by

$$N_i(L, t) = Lk_p Z_i'(L)T_i(t) + Lc_p Z_i'(L)\dot{T}_i(t). \tag{30}$$

At a free end, the normal force equals zero for all t and, therefore, $Z_i'(L) = 0$. The nontrivial solution of this equality gives values for μ_i

$$N_i(L, t) = 0 \;\rightarrow\; \mu_i = \frac{i\pi}{2L}, \qquad i = 1, 3, 5, \ldots. \tag{31}$$

Thus, taking the boundary conditions into account $Z_i(z)$ can be determined up to a constant

$$Z_i(z) = B_i\sin\left(\frac{i\pi}{2L}z\right), \qquad i = 1, 3, 5, \ldots. \tag{32}$$

For $i = 1, 3, 5, \ldots$, $|Z_i(L)|$ is maximal, which corresponds with a trough for the elongation $y_i(t)$. Note that for $i = 2, 4, 6, \ldots$, $Z_i(L) = 0$, which corresponds with $y_i(t) = 0$, i.e., with a node for the elongation of the PEA.

We continue with the evaluation of the eigenfrequencies and the relative dampings of the eigenmodes, i.e., we consider (27). The well-known general differential equation for linear time-invariant second order systems is

$$\ddot{T}_i + 2\xi_i\omega_{u,i}\dot{T}_i + \omega_{u,i}^2 T_i = 0 \tag{33}$$

where $\omega_{u,i}$ stands for the undamped, or natural, eigenfrequency and ξ_i denotes the relative damping. By comparing (27) with (33) and using (31), these characteristics can be derived to be

$$\omega_{u,i} = \frac{i\pi}{2}\sqrt{\frac{k_p}{m_p}}, \qquad i = 1, 3, 5, \ldots \tag{34}$$

$$\xi_i = \frac{i\pi}{4}\frac{c_p}{\sqrt{k_p m_p}}, \qquad i = 1, 3, 5, \ldots. \tag{35}$$

From this result, we conclude that even for small values of c_p, the higher modes are strongly damped. Note that for $i = 2, 4, 6, \ldots$, these characteristics can also be calculated, which gives eigenfrequencies corresponding to eigenmodes with $y_i(t) = 0$.

The roots of (33) are given by

$$-\xi_i\omega_{u,i} \pm j\omega_{d,i}, \qquad \omega_{d,i} = \omega_{u,i}\sqrt{1 - \xi_i^2} \tag{36}$$

where it is assumed that $\xi_i < 1$, which is not true for large i, as will be clear from (35). Furthermore, $\omega_{d,i}$ are the damped eigenfrequencies, which are the frequencies that actually appear. Substitution of (34) and (35) in (36) gives, for i odd, the poles of the transfer function $M(s) = y(s)/(F_p(s) - F_e(s))$, where s is the Laplace variable and where y, as defined before, is the elongation of the PEA. In case of a fixed end at $z = 0$, we have $y(s) = v(L, s)$. For i, even we obtain the zeros of $M(s)$. It can be proven that the poles and zeros for which $\xi_i \leq 1$ lie on a circle with center $(-k_p/c_p, 0)$ and radius k_p/c_p. The other poles and zeros are located on the real axis. In Fig. 6, the pole–zero pattern of the mechanical model of a PEA with $k_p = 4 \times 10^7$ N/m, $c_p = 1 \times 10^2$ kg/s, and $m_p = 0.1$ kg is presented.

In a Bode plot of $M(s)$, the poles and zeros appear as peaks and valleys, respectively. In Fig. 7, a Bode plot is presented for a PEA with m_p and k_p, as in the previous plot, but with $c_p = 10$ kg/s in order to have well-visible peaks and valleys.

For i odd, as well as even, the corresponding eigenmode is a standing wave in the spatial domain. For a fixed time t, these

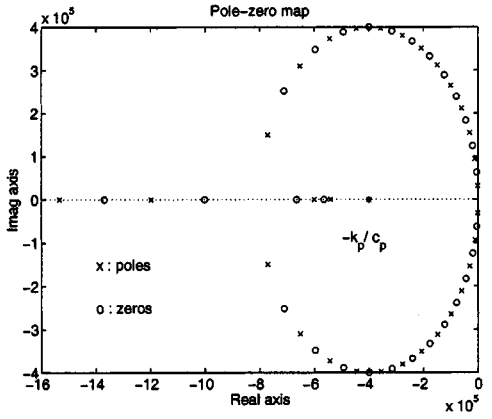

Fig. 6. Pole–zero pattern of a PEA.

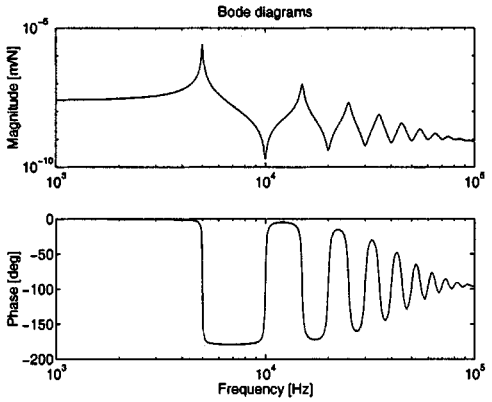

Fig. 7. Bode plot of a PEA.

TABLE II
SUBSEQUENT EIGENMODES FOR FIXED t TOGETHER WITH THE CORRESPONDING DAMPED EIGENFREQUENCIES AND POLE–ZERO INDICATIONS

i	Eigenmode	Damped eigenfreq.	pole/zero
1	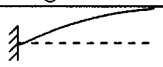	$\frac{\pi}{2}\sqrt{\frac{k_p}{m_p}-\left(\frac{\pi}{2}\frac{c_p}{m_p}\right)^2}$	pole
2	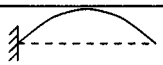	$\pi\sqrt{\frac{k_p}{m_p}-\left(\pi\frac{c_p}{m_p}\right)^2}$	zero
3	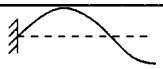	$\frac{3\pi}{2}\sqrt{\frac{k_p}{m_p}-\left(\frac{3\pi}{2}\frac{c_p}{m_p}\right)^2}$	pole
4	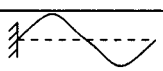	$2\pi\sqrt{\frac{k_p}{m_p}-\left(2\pi\frac{c_p}{m_p}\right)^2}$	zero
⋮	⋮	⋮	⋮

waves are shown in Table II together with the corresponding damped eigenfrequencies and pole/zero indications. Of course, we deal with longitudinal waves, but for visualization reasons, they are shown as transversal waves.

Having determined the poles and zeros, we can give a transfer function description of the mechanical behavior of a PEA

$$M(s)=\frac{y(s)}{F_p(s)-F_e(s)}=\frac{N_p(s)}{D_p(s)} \tag{37}$$

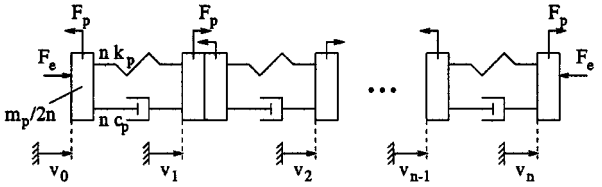

Fig. 8. Chain of mass-spring-damper systems as an approximate mechanical model of the PEA.

with the polynomials $N_p(s)$ and $D_p(s)$ in a nonmonic form given by

$$N_p(s)=\prod_{i=1}^{\infty}\frac{m_p}{\mu_{2i}^2L^2}s^2+c_ps+k_p \tag{38}$$

$$D_p(s)=\prod_{i=1}^{\infty}\frac{m_p}{\mu_{2i-1}^2L^2}s^2+c_ps+k_p. \tag{39}$$

Approximations of arbitrary order can be made by taking an arbitrary number of poles and zeros into account. We deal with a physical system and, therefore, in the approximation the number of pole pairs should exceed the number of zero pairs with one. For such approximations, it is easy to see that the static gain of the transfer function is $1/k_p$. This corresponds with the PDE of (22). The approximate models obtained in this way are called modal approximation models.

Finite-difference approximation models can be obtained by numerical approximation of the position derivatives in the PDE. The numerical approximation of the second derivative with respect to z is

$$\frac{\partial^2 v}{\partial z^2}=\frac{v_{l+1}-2v_l+v_{l-1}}{h^2} \tag{40}$$

where $v_l=v(z_l,t)$ with $z_l=lh$ for $l=0,1,\ldots,n$. Substitution in (22) and introduction of $n=L/h$ after some simple manipulations gives

$$nk_p(v_{l+1}-v_l)-nk_p(v_l-v_{l-1})+nc_p(\dot v_{l+1}-\dot v_l) -nc_p(\dot v_l-\dot v_{l-1})=\frac{m_p}{n}\ddot v_l,\qquad l=1,\ldots,n-1. \tag{41}$$

Physically, this corresponds with a chain of mass-spring-damper systems, as in Fig. 8. Here, the ends of the PEA are modeled by one-half of the mass of the other elements. Note that (41) does not give us the equations of motion for these ends of the PEA. These can easily be derived to be

$$nk_p(v_{l+1}-v_l)+nc_p(\dot v_{l+1}-\dot v_l)-F_p+F_e=\frac{m_p}{2n}\ddot v_l,\qquad l=0 \tag{42}$$

$$-nk_p(v_l-v_{l-1})-nc_p(\dot v_l-\dot v_{l-1})+F_p-F_e=\frac{m_p}{2n}\ddot v_l,\qquad l=n. \tag{43}$$

The symmetric model of Fig. 8 reflects the practical situation, where the PEA does not show a preferable direction. The element consisting of a spring and damper and at both sides half of an elements mass can be considered as an elementary element of

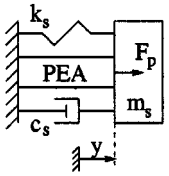

Fig. 9. Total system of PEA and stage where the latter is a mass-spring-damper system.

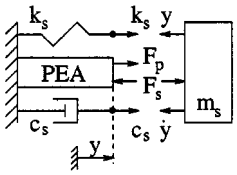

Fig. 10. Visualization of the interaction force between PEA and stage.

the chain. Note that the transduced forces cancel out at the connection between two elements. Thus, macroscopically there are, just as in Section II, only forces at the first and last electrode. The advantage of finite-difference approximation models, with respect to the modal approximation models, is the flexibility with respect to different boundary conditions. The boundary conditions can be incorporated in the equations for the ends of the PEA, i.e., in (42) and (43).

The approximation of the PDE converges to the PDE for $n \to \infty$. By choice of n, approximations of arbitrary order can be made.

V. Mechanical Model of a Piezo-Actuated Positioning Mechanism

Up to now, we have considered a PEA as a standalone element. In practice, however, a PEA is most often used as an actuator for positioning mechanisms. We restrict ourselves to positioning mechanisms that are accurately modeled by a simple mass-spring-damper system. In the following, we use "stage" for positioning mechanism. In Fig. 9, the total system of PEA and stage is presented. At one side, the PEA is fixed and at the other side, it is connected to the stage of which m_s, c_s, and k_s are the mass, damping, and stiffness, respectively.

The interaction force between PEA and stage, i.e., the force acting on the PEA due to the presence of the stage and vice versa, is denoted by F_s and may be derived from Fig. 10.

The expression for the interaction force is

$$F_s = m_s\ddot{y} + c_s\dot{y} + k_s y. \tag{44}$$

After Laplace transformation, we may write

$$F_s(s) = D_s(s)y(s) \quad D_s(s) = m_s s^2 + c_s s + k_s. \tag{45}$$

In [7], the presence of a stage is accounted for in a block diagram for the case that the mechanical model of the PEA is a mass-spring-damper system. A similar block diagram is presented in Fig. 11. Note that the stage stiffness, damping, and mass work as position, velocity, and acceleration feedback, respectively.

Comparison of Figs. 3 and 10 or (37) and Fig. 11 teaches us that F_s influences the PEA behavior in a similar way as an externally applied force. The only difference is that F_s depends

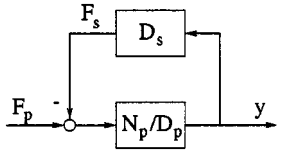

Fig. 11. Block diagram of the mechanical model of PEA and stage together.

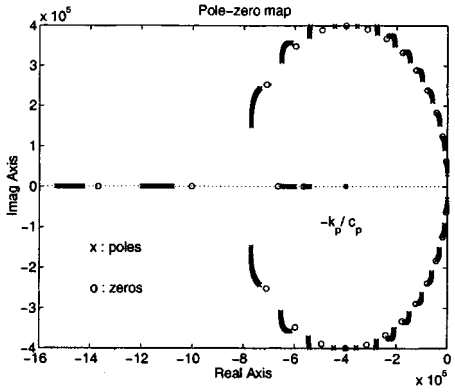

Fig. 12. Root locus for increasing value of the stage stiffness ($0 < k_s < 50\,k_p$).

on the elongation of the PEA. The mechanical relation between F_p and y can be derived to be

$$y(s) = \frac{N_p(s)}{N_p(s)D_s(s) + D_p(s)}\,F_p(s). \tag{46}$$

It may be seen the numerator polynomial has not changed, despite the fact that we have a stage. Physically this can be understood from the fact that, in case of a zero, the elongation $y(t) = 0$, which means that the stage is at rest. Therefore, the zeros are invariant for the stage properties.

In order to determine the new pole locations, we separately consider the cases where we have only stage stiffness, only stage damping, and only stage mass. In the case of only stage stiffness k_s, we have the denominator polynomial $N_p(s)k_s + D_p(s)$. The analogy with a root locus problem is to be remarked upon. A first basic rule for root locus is that, for $k_s = 0$, the poles coincide with the original poles. A second basic rule is that, for $k_s \to \infty$, the poles tend to the zeros. The remaining poles tend to infinity. In our case, there are infinitely many poles and zeros. However, as mentioned in the previous section, in an approximation, the number of pole pairs exceeds the number of zero pairs by one. In Fig. 12, the root locus for $0 < k_s < 50\,k_p$ is shown. Clearly, the poles tend to zeros. However, one of the poles at the top (and at the bottom) of the circle tends to infinity. This is not visible yet due to the not large enough values of k_s, although even $k_s = k_p$ is already unrealistically large.

In case of only stage damping, the denominator polynomial is given by $N_p(s)sc_s + D_p(s)$, where s can be considered as an extra zero in the origin, to which a pole tends for increasing c_s. Thus, in this case, only one pole tends to infinity. The root locus for $0 < c_s < 50\,c_p$ is shown in Fig. 13.

When we only have stage mass, the denominator polynomial is given by $N_p(s)s^2m_s + D_p(s)$, where s^2 can be considered as two extra zeros in the origin, to which two poles tend for

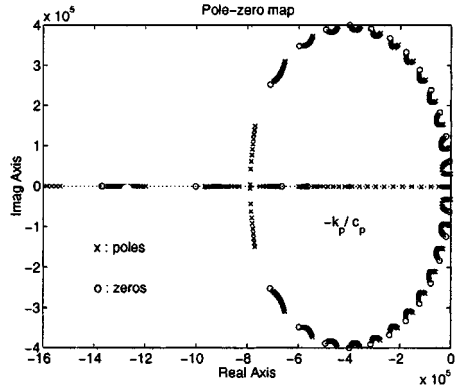

Fig. 13. Root locus for increasing value of the stage damping ($0 < c_s < 50\,c_p$).

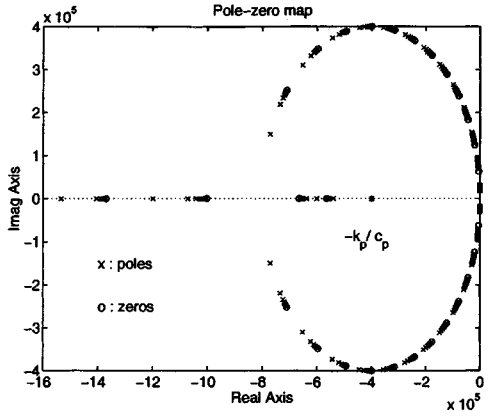

Fig. 14. Root locus for increasing value of the stage mass ($0 < m_s < m_p$).

increasing m_s. In this case, none of the poles tends to infinity. In Fig. 14, the root locus for $0 < m_s < m_p$ is shown.

For increasing m_s, the poles seem to stay on the circle. Furthermore, the effect of m_s is strong because already for very small values the pole locations change significantly. Note that the first pole pair tends to the origin, i.e., the first eigenfrequency decreases. Typically, the first eigenfrequency of a PEA is between 5–10 kHz. The reason for this is its relatively high stiffness and its relatively low mass. By stage design, we, therefore, usually aim at decreasing this eigenfrequency or, in other words, the bandwidth of the system. This enhances digital control of the system. Thus, the effect of increasing m_s is favorable.

For increasing k_s, the effect is less strong than for m_s. Moreover, because of the already high stiffness of the PEA, we do not aim at a stiff stage design. Thus, in practice, the influence of the stage stiffness on the pole locations is negligible.

The structural damping of a PEA is very small and, therefore, with stage design, we aim at adding damping in order to obtain well-damped behavior of the total system. Note that, for increasing c_s, the poles tend to the zeros located on the other side of the original poles than for increasing m_s.

Simulations showed that, especially for the higher eigenfrequencies, the effect of increasing m_s is so strong that it dominates the effect of c_s. For the first pole pair, the effects of both m_s and c_s have to be taken into account. Thus, both undamped eigenfrequency and relative damping of this pole pair can be

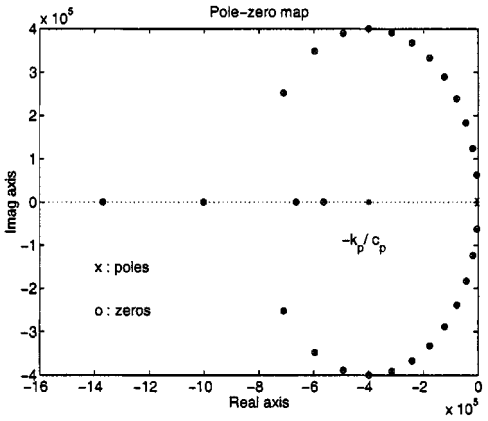

Fig. 15. Pole–zero pattern of the mechanical model of PEA and stage together with well-designed stage properties.

designed favorably. Summarizing, for a practical stage design, the poles tend to the unchanged zeros, which means that poles and zeros cancel out in a transfer function. Therefore, in a Bode plot, no peaks and valleys are to be observed. The first pole pair could be designed to our wish and, therefore, in a Bode plot, this one is visible as the cutoff frequency. A good approximation of the relation between F_p and y in differential form is

$$m\ddot{y} + c\dot{y} + ky = F_p \tag{47}$$

with

$$\begin{aligned} m &= \frac{m_p}{\mu_1^2 L^2} + m_s = \frac{4m_p}{\pi^2} + m_s \\ c &= c_p + c_s \\ k &= k_p + k_s. \end{aligned} \tag{48}$$

This approximate model reflects the influence of the stage on the first eigenmode. We aim at an undamped eigenfrequency of 1 kHz and a relative damping of $(1/2)\sqrt{2}$. The value of k_s is designed such that it is considerably smaller than the PEA stiffness, but still realistic for a mechanical system, i.e., $k_s = 5 \times 10^6$ N/m. Since $k_p = 4 \times 10^7$ N/m, the overall stiffness is $k = 4.5 \times 10^7$ N/m. The value of m_s is designed to achieve the cutoff frequency of approximately 1 kHz. Since $m_p = 0.1$ kg, it follows that we need $m_s = 1.1$ kg. Furthermore, c_s is designed such that the favorable relative damping is obtained. Since the damping in the PEA is estimated to be $c_s = 1 \times 10^2$ kg/s, it follows that we need $c_s = 1 \times 10^4$ kg/s. In Fig. 15, the pole–zero pattern of the mechanical model of a PEA and a stage together is presented, with the stage properties as derived above, i.e., a well-designed stage. Note that all pole pairs, except for the first pair, indeed approximately cancel all zero pairs.

In Fig. 16, the Bode plot of the total mechanical model of PEA and stage is shown together with the Bode plot of the approximate model. Only at 1×10^4 Hz, i.e., the frequency that corresponds with the first valley/zero, a small difference is visible. Here, the pole does not perfectly cancel the zero.

With a well-designed stage, the behavior of the total mechanical system of PEA and stage practically equals that of a single mass-spring-damper system. The model simplification is considerable.

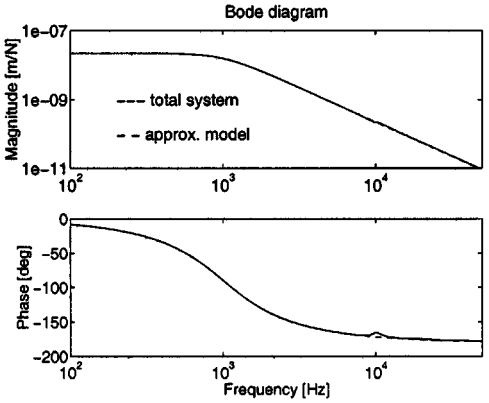

Fig. 16. Bode plots of the mechanical model of PEA and stage together with well-designed stage properties and of the approximate mechanical model.

Finally, we briefly want to consider the design of the positioning mechanism that has the desired properties we derived above. The low stiffness we aimed at can be achieved in a construction with leaf springs. The required mass can be achieved in a metal construction. However, in such a metal construction, there is almost no intrinsic damping. To introduce this, we could use a system based on the concept of Eddy current damping. This system consists of a copper ring attached to the fixed world and a ferromagnetic backplane with a number of strong permanent magnets attached to the moving mass. By adjusting the gap between the copper plate and the magnets, the damping constant can be tuned to our desired value. We remark that this construction may indeed be accurately modeled by a simple mass-spring-damper system, as we assumed earlier. The mass is concentrated in the moving part, the stiffness, or in fact weakness, is concentrated in the leaf springs, and preliminary experiments with the Eddy current damping system show that it gives linear damping.

VI. Voltage and Charge Steering Configurations

As we have learned from Section II, two ways of electrical steering may be distinguished, namely, voltage and charge steering. A voltage-steering configuration is simple, but in this case, hysteresis is present in the input/output behavior. A charge-steering configuration is more complicated, but once established, hysteresis does not play a role anymore.

For maximum elongation, the voltage difference over a high-voltage PEA has to be in the order of 1000 V for almost any commercially available type. Most piezo-actuated mechanisms are computer controlled and, thus, the maximum steering voltage is limited to much smaller values. The use of high-voltage amplifiers is, therefore, unavoidable.

In the remainder of this section, we design the basic, or principle, configurations for both voltage steering (Section VI-A) and charge steering (Section VI-B).

A. Voltage-Steering Configuration

As mentioned at the beginning of this section, the configuration for voltage steering is simple. The principle is shown in Fig. 17, where u represents the voltage generated by the computer and B signifies the amplification factor.

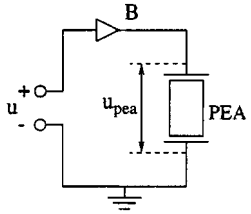

Fig. 17. Basic configuration for voltage steering.

As a relation for the maximum voltage difference over the PEA, we have

$$Bu_{\max} = u_{pea,\max}. \tag{49}$$

This equality is considered to be a design rule. For maximum elongation, $u_{pea,\max} = 1000$ V. The design variables B and $u_{\max}$ should be chosen such that this is possible. Note that the design constraints are the electronic possibilities, i.e., the design variables have to be chosen such that the configuration is practically realizable.

For this configuration, the charge in the PEA clearly depends on the PEAs impedance, which is partly determined by the hysteresis effect (Fig. 3).

B. Charge-Steering Configuration

In Section II, we have argued that, in case of charge steering, the hysteresis effect is not encountered. In the early 1980's, this result has independently been reported in [4] and [17]. A charge-steering configuration has to be designed such that the charge applied to the PEA is independent of the PEAs impedance. This is completely analog to a current-steering configuration, which has to be designed such that the current applied to a certain impedance is independent of that impedance.

In [17], a current source is used as a basis for charge steering. A more direct approach is followed in [4], where a simple configuration is proposed consisting of a voltage source, an operational amplifier (opamp), an external capacitance, and a high-voltage amplifier. In [16] and [21], the same basic configuration is introduced. Especially in [16], it is clearly noted that this simple configuration has two apparent drawbacks: both sides of the PEA are floating with respect to ground and the configuration is very sensitive to opamp bias current. In [21], various countermeasures are proposed to overcome these problems.

Here, we only consider the basic configuration, which is shown in Fig. 18. u_a, u_b, and u_c are the input voltages and the output voltage of the opamp, B_1 and B_2 are high-voltage amplifiers, and C_e is the external capacitance.

As for the case of voltage steering, we want to derive design rules. In the analysis, we assume to have an ideal opamp, i.e., $u_a = u_b$ and $i_b = 0$. From Fig. 18, it is clear that $u_a = u$ and, thus, $u_b = u$. Since $i_b = 0$, the charge q in the PEA equals that in C_e, which can easily be derived to be

$$q = \frac{C_e}{B_2} u. \tag{50}$$

thus, it can now already be concluded that the charge applied to the piezo is independent of the piezo impedance. However, there are more requirements that have to be met. Namely, the voltage

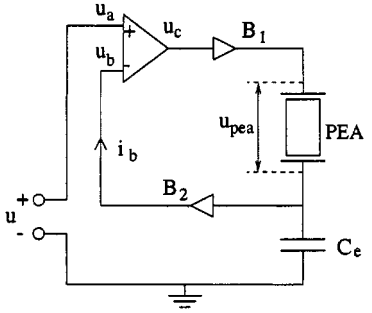

Fig. 18. Basic configuration for charge steering.

difference over the piezo should be able to attain 1000 V in order to achieve maximum elongation.

From (12), it can easily be concluded that the maximum value of u_h is attained for the maximum value of q and is given by $u_{h,\max} = (1/a)q_{\max}$. From (6) and (7), we can also derive the maximum value of u_p as a function of the maximum values of q and y to be given by $u_{p,\max} = (1/C)q_{\max} - (T_{\rm em}/C)y_{\max}$. Substitution of the previous results in (4) then gives the maximum value for the voltage over the PEA, i.e., $u_{pea,\max} = ((a+C)/(aC))q_{\max} - (T_{\rm em}/C)y_{\max}$. A relation for $q_{\max}$ as a function of $u_{pea,\max}$ and $y_{\max}$ can easily be obtained from this relation. Using (50), another relation for $q_{\max}$ may be derived, i.e., $q_{\max} = (C_e/B_2)u_{\max}$. From these two relations for $q_{\max}$, the following design rule can be derived:

$$\frac{C_e}{B_2}u_{\max} = \frac{aC}{a+C}\left(u_{pea,\max} + \frac{T_{\rm em}}{C}y_{\max}\right). \tag{51}$$

The right-hand side only contains PEA properties, while the left-hand side contains the design variables, i.e., the variables from the charge-steering circuit of Fig. 18. These are chosen such that they fit with a specific PEA.

The voltage over the PEA is given by $u_{\rm pea} = B_1u_c - (1/B_2)u$. When we think of u_c as a constant factor times u, it can easily be seen that the maximum value for $u_{\rm pea}$ is attained for maximum input u. The second design rule is now given by

$$B_1u_{c,\max} = u_{pea,\max} + \frac{1}{B_2}u_{\max}. \tag{52}$$

The right-hand side contains a PEA property and design variables that have been chosen according to the first design rule of (51). The left-hand side contains the other two design variables.

Finally, we state that, as in the case of voltage steering, the five design variables C_e, B_2, $u_{\max}$, B_1, and $u_{c,\max}$ have to be chosen based on electronic possibilities in order to obtain a practically realizable design.

VII. Total Model for the Case of Charge Steering

In this section, we derive the total model of a piezo-actuated positioning mechanism for the case of charge steering. We recall that, for this case of electric steering, the hysteresis effect does not play a role. In Fig. 9, we presented the total system of PEA and stage.

Of the complete set of electromechanical equations (4)–(9), the following play a role in the case of charge steering:

$$q = Cu_p + q_p \tag{53}$$

$$q_p = T_{\rm em}y \tag{54}$$

$$F_p = T_{\rm em}u_p \tag{55}$$

$$m\ddot{y} + c\dot{y} + ky = F_p \tag{56}$$

where the mechanical model is equal to (47), i.e., the mechanical model of a well-designed piezo-actuated positioning mechanism. After simple manipulations, the following equation may be obtained:

$$m\ddot{y} + c\dot{y} + k_oy = \beta_oq \tag{57}$$

where k_o and β_o are as defined in [7]

$$k_o = k + \frac{T_{\rm em}^2}{C} \tag{58}$$

$$\beta_o = \frac{T_{\rm em}}{C}. \tag{59}$$

The index "o" is used because the case of charge steering in Section II is also referred to as the galvanically open situation.

Using the relation for charge steering (50), i.e., the relation between the input voltage generated in the computer and the charge in the PEA, the total model for the case of charge steering can easily be derived to be given by

$$m\ddot{y} + c\dot{y} + k_oy = \beta_o\frac{C_e}{B_2}u. \tag{60}$$

Summarizing, by changing traditional voltage steering for charge steering and by proper design of the positioning mechanism, it is possible to bypass both the hysteresis effect and the distributed parameter character. Therefore, the total model of a piezo-actuated positioning mechanism for the case of charge steering is significantly simplified with respect to the PEA model, as presented in Sections II–IV. The obtained model is very suitable as a basis for controller design.

VIII. Conclusion

In this paper we have, based on [11], formulated an electromechanical model for the PEA. What we added is the use of a nonlinear first-order differential equation to describe the hysteresis effect and the use of a PDE, including structural damping, to describe the mechanical behavior.

Eigenmodes and their corresponding eigenfrequencies and relative dampings associated with the mechanical behavior have been analytically determined. The poles and zeros of the mechanical model lie on a circle of which the center point and radius have been determined. In a Bode plot, the peaks and valleys associated with the poles and zeros appear alternatingly.

Based on a transfer-function representation of the mechanical model of the PEA, the influence of a positioning mechanism on the overall behavior of a PEA and a positioning mechanism together has been considered. Determining this influence can be considered as a root locus problem. Except for the first pole pair, the poles of the overall mechanical model tend to the unchanged zeros of the model. This has been shown in pole–zero

maps. For the transfer function description of the overall mechanical model this means that, except for the first pole pair, all poles and zeros cancel out. The first pole pair can be designed to our wish and, therefore, the overall mechanical system can be designed such that it practically equals a single mass-spring-damper system with favorable eigenfrequency and relative damping.

Contrary to the case of voltage steering, hysteresis does not play a role in the case of charge steering. The basic configurations for both cases of electrical steering have been presented here.

For the case of charge steering, we derived the total model of a piezo-actuated positioning mechanism. This model is dominated by the mechanical model, which could be designed favorably. Therefore, this model gives a broad range of possibilities for model-based controller design.

Finally, we repeat the most important conclusion. By changing traditional voltage steering for charge steering and by proper design of the positioning mechanism, it is possible to bypass the hysteresis effect and the distributed parameter character of a PEA, respectively. Therefore, the total model of a piezo-actuated positioning mechanism can be significantly simplified. The obtained model is very suitable as a basis for controller design.

REFERENCES

[1] R. Banning, W. L. de Koning, J. M. T. A. Adriaens, and K. R. Koops, "State-space analysis and identification for a class of hysteretic systems," *Automatica*, to be published.

[2] B. M. Chen, T. H. Lee, C. C. Hang, Y. Guo, and S. Weerasooriya, "An H_∞ almost disturbance decoupling robust controller design for a piezoelectric bimorph actuator with hysteresis," *IEEE Trans. Contr. Syst. Technol.*, vol. 40, pp. 160–174, Mar. 1999.

[3] B. D. Coleman and M. L. Hodgdon, "A constitutive relation for rate-independent hysteresis in ferromagnetically soft materials," *Int. J. Eng. Sci.*, vol. 24, pp. 897–919, 1986.

[4] R. H. Comstock, "Charge control of piezoelectric actuators to reduce hysteresis effects," U.S. Patent 4 263 527, 1981.

[5] D. Croft and S. Devasia, "Hysteresis and vibration compensation for piezoactuators," *AIAA J.*, vol. 21, pp. 710–717, 1998.

[6] D. Croft, D. McAllister, and S. Devasia, "High-speed scanning of piezo-probes for nano-fabrication," *J. Manufact. Sci. Eng.*, vol. 120, pp. 617–622, 1998.

[7] W. L. de Koning, J. M. T. A. Adriaens, and R. Banning, "Physical modeling of piezoelectric actuators for control purposes," in *Proc. IFAC Motion Control Workshop*, 1998, pp. 37–42.

[8] M. Dimmler, U. Holmberg, and R. L. Longchamp, "Hysteresis compensation of piezo-actuators," in *Proc. 5th European Control Conf.*, 1999, CDROM paper f0700.

[9] P. Ge and M. Jouaneh, "Modeling hysteresis in piezoceramic actuators," *Precision Eng.*, vol. 17, pp. 211–221, 1995.

[10] ——, "Tracking control of a piezoceramic actuator," *IEEE Trans. Contr. Syst. Technol.*, vol. 4, pp. 209–216, May 1996.

[11] M. Goldfarb and N. Celanovic, "Modeling piezoelectric stack actuators for control of micromanipulation," *IEEE Contr. Syst. Mag.*, vol. 17, pp. 69–79, 1997.

[12] S.-B. Jung and S.-W. Kim, "Improvement of scanning accuracy of PZT piezoelectric actuators by feed-forward model-reference control," *Precision Eng.*, vol. 16, pp. 49–55, 1994.

[13] C. J. Li, H. S. M. Beigi, S. Li, and J. Liang, "Nonlinear piezo-actuator control by learning self-tuning regulator," *J. Dynamic Syst., Meas., Contr.*, vol. 115, pp. 720–723, 1993.

[14] C. Liang, F. P. Sun, and C. A. Rogers, "Investigation of the energy transfer and consumption of adaptive structures," in *Proc. 31st Decision Contr. Conf.*, 1992, pp. 1791–1796.

[15] D. R. Madill and D. Wang, "Modeling and L2-stability of a shape memory alloy position control system," *IEEE Trans. Contr. Syst. Technol.*, vol. 6, pp. 473–481, July 1998.

[16] J. A. Main, E. Garcia, and D. V. Newton, "Precision position control of piezoelectric actuators using charge feedback," *J. Guidance, Contr., Dynam.*, vol. 18, pp. 1095–1073, 1995.

[17] C. V. Newcomb and I. Flinn, "Improving the linearity of piezoelectric ceramic actuators," *Electron. Lett.*, vol. 18, pp. 442–444, 1982.

[18] M. Pozzi and T. King, "Dynamic characteristics of piezoelectric multilayer stack actuators," in *Proc. 2nd Int. Recent Advances Mechatron. Conf.*, 1999, pp. 461–466.

[19] J. Schäfer and H. Janocha, "Compensation of hysteresis in solid-state actuators," *Sens. Actuators A, Phys.*, vol. 49, pp. 97–102, 1995.

[20] *An American National Standard: IEEE Standard on Piezoelectricity*, ANSI/IEEE Standard 176-1987, 1987.

[21] K. Takata, M. Okumura, S. Fukuhara, T. Morimura, S. Hosaka, and S. Hosoki, "Piezoelectric actuator control apparatus," U.S. Patent 4 841 191, 1989.

[22] S. Yang and W. Huang, "Dynamic analysis of piezoelectric elements," *Rev. Sci. Instrum.*, vol. 66, pp. 4157–4160, 1995.

[23] Q. Zhou, P. Kallio, and H. N. Koivo, "Nonlinear system identification of a micromanipulator," in *Proc. 2nd Int. Recent Advances Mechatron. Conf.*, 1999, pp. 467–472.

Han J. M. T. A. Adriaens was born in Geldrop, The Netherlands, in 1972. He received the M.Sc. degree in mechanical engineering from the Eindhoven University of Technology, Eindhoven, The Netherlands, in 1996, and the Ph.D. degree in applied mathematics from the Delft University of Technology, Delft, The Netherlands, in 2000.

He is currently with ASM Lithography, Veldhoven, The Netherlands, where machines for semiconductor manufacturing are developed and produced. His main research interest is in applied mathematics, with a focus on nonlinear systems and control, and on measurement systems.

Willem L. de Koning was born in Leiden, The Netherlands, in 1944. He received the M.Sc. and Ph.D. degrees in electrical engineering from the Delft University of Technology, Delft, The Netherlands in 1975 and 1984, respectively.

From 1969 to 1975, he was a Research Engineer of power electronics and control in the Department of Electrical Engineering, Delft University of Technology. From 1975 to 1987, he was an Assistant Professor of process dynamics and control in the Department of Applied Physics, Delft University of Technology. Since 1987, he has been an Associate Professor of mathematical system theory in the Department of Information Technology and Systems, Delft University of Technology. He has also held a visiting position at the Florida Institute of Technology, Melbourne. His research interests include control of distributed-parameter systems, reduced-order control, adaptive predictive control, digital optimal control, and applications.

Reinder Banning was born in Leeuwarden, The Netherlands, in 1966. He received the M.Sc. degree in applied mathematics from the University of Twente, Twente, The Netherlands, in 1989, and the Ph.D. degree in electronic and electrical engineering from Strathclyde University, Strathclyde, Scotland, in 1993.

He held a research assistantship at Strathclyde University. Since 1993, he has been an Assistant Professor in systems and control in the Department of Applied Physics, Delft University of Technology, Delft, The Netherlands. His research interests include optimal control, nonlinear systems and control, nanometer positioning, and stochastic systems.